**Supplemental Figures.**

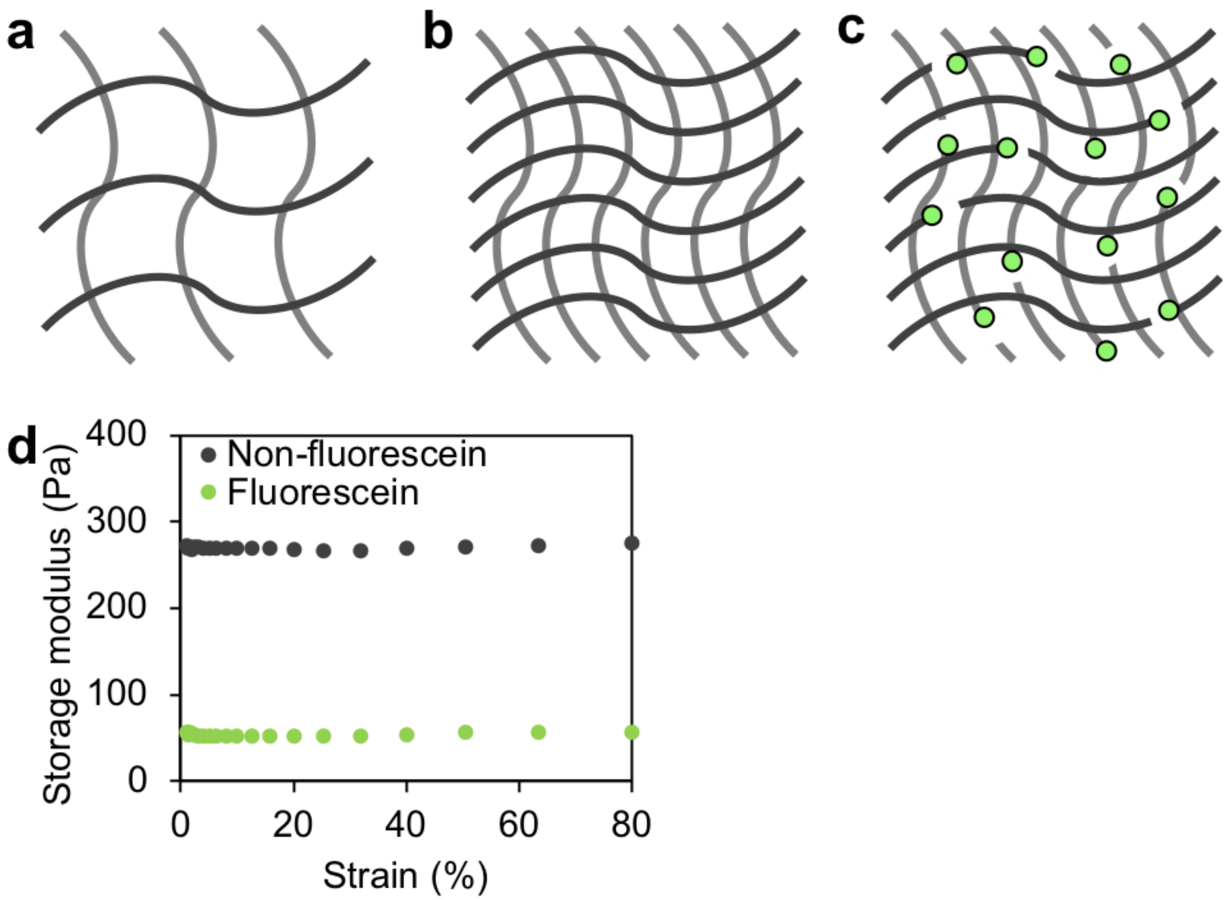


**Supplementary Figure 1.** Polyacrylamide matrices that are (**a**) low polymer content and soft; (**b**) high polymer content and stiff; and (**c**) high polymer content, but reduced stiffness due to incorporation of fluorescein o-methacrylate, a chain-terminating monomer. (**d**) Bulk shear rheology on polyacrylamide hydrogels polymerized with fluorescein o-methacrylate monomers demonstrate that for 100 μg/mL of fluorescein methacrylate, the stiffness of polyacrylamide matrices are reduced by five-fold compared to non-fluorescent hydrogels. The modified hydrogels retain their mechanical modulus properties over a large deformation range.

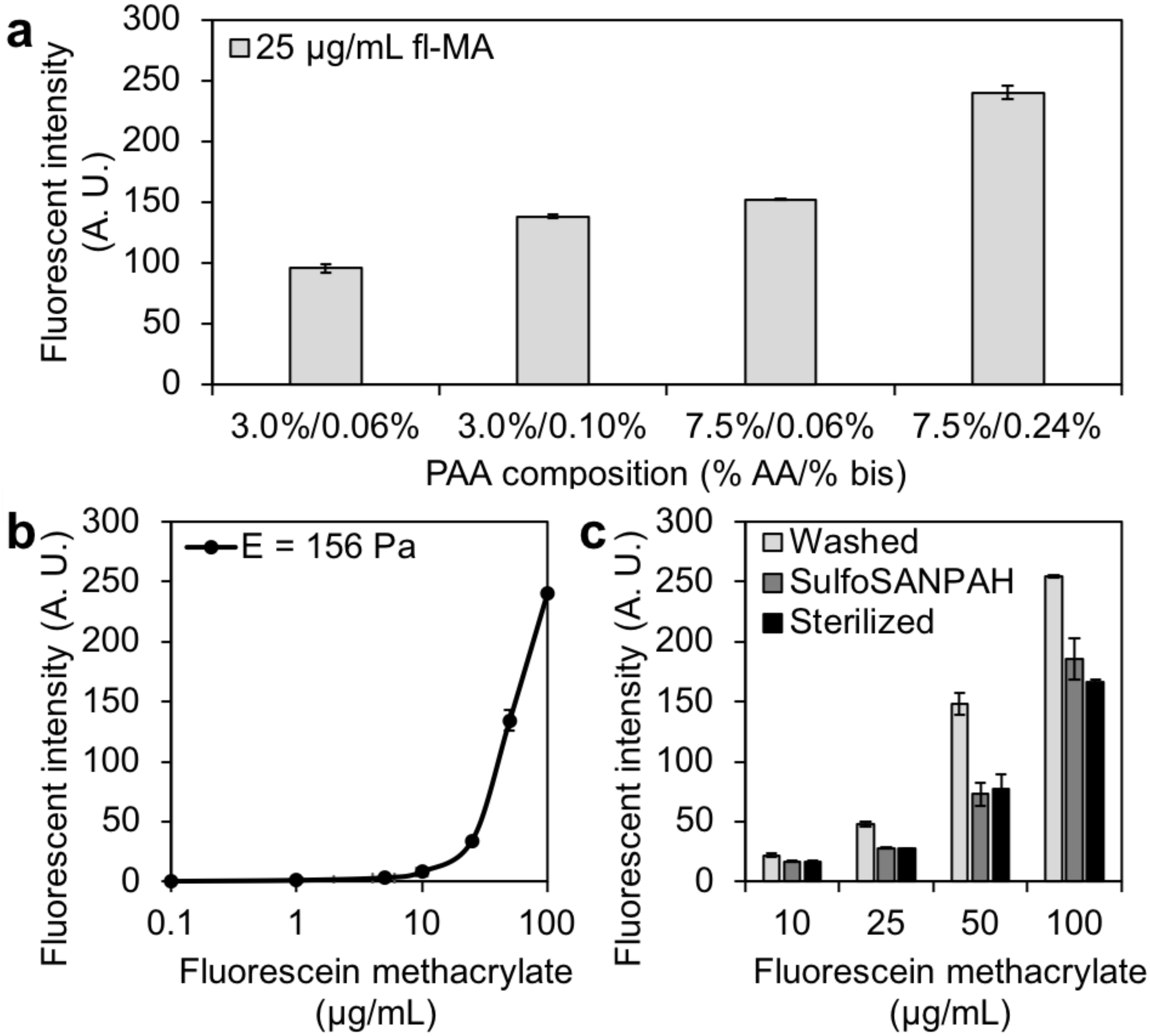


**Supplementary Figure 2.** Characterization of MSG fluorescence through co-polymerization with fluorescein methacrylate (fMA) monomers. Hydrogel fluorescent intensity depends on (**a**) MSG modulus, and (**b**) fMA concentration, as more polymerized fluorescent monomer results in higher fluorescent intensity. (**c**) Surface functionalization and sterilization steps further reduce the fluorescent intensity after the hydrogel is washed thoroughly. Data reported as mean ± standard deviation. These results indicate that fluorescein methacrylate is incorporated stably into the polymer backbone, allowing persistent labelling during cell culture experiments.

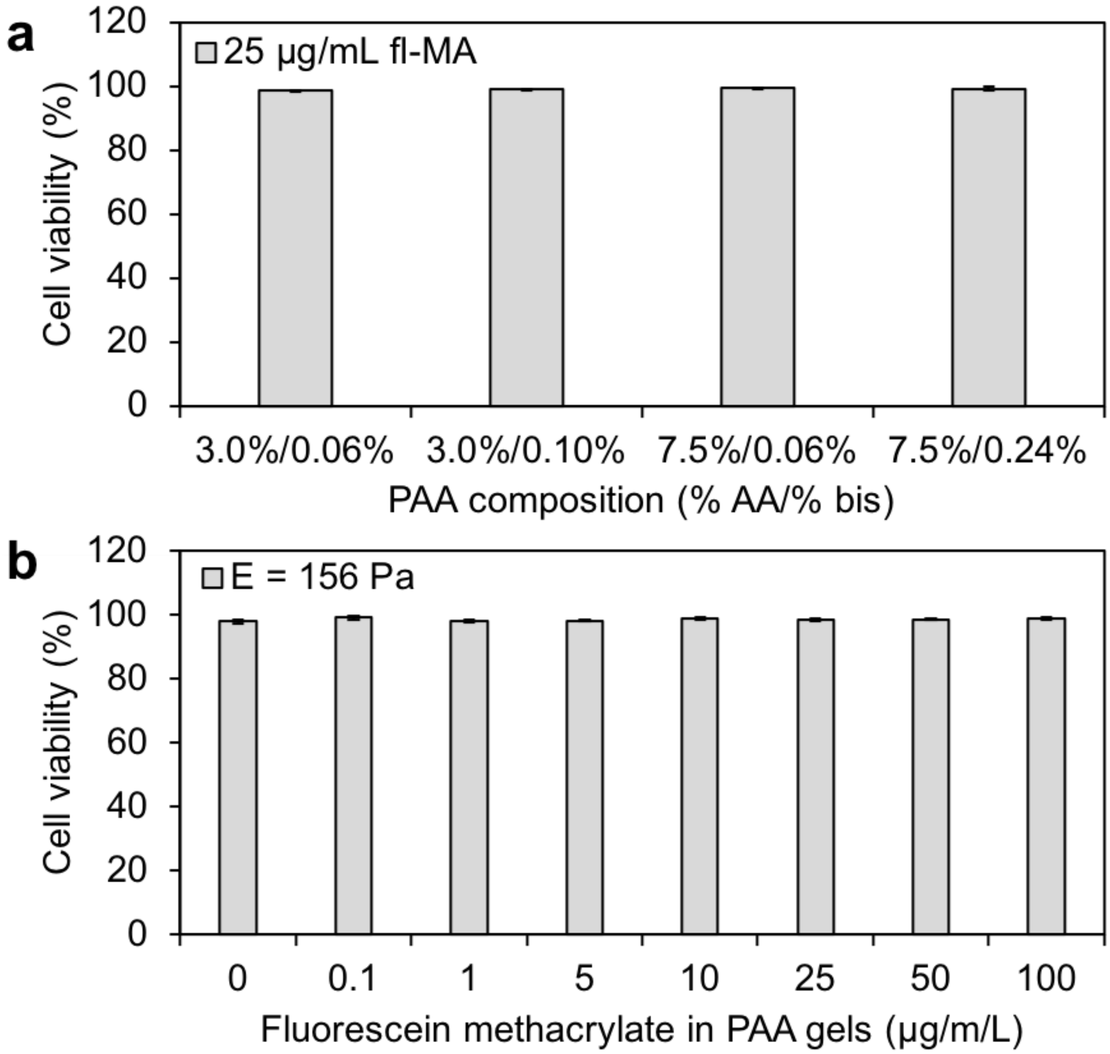


**Supplementary Figure 3.** Confirmation of cell viability in polyacrylamide hydrogels modified with fluorescein methacrylate monomers. HS-5 human bone marrow fibroblast cells cultured on polyacrylamide hydrogel formulations remained viable after 24 hours independent of (**a**) hydrogel modulus, and (**b**) fluorescent methacrylate concentration within the hydrogel. Data reported as mean ± standard deviation.

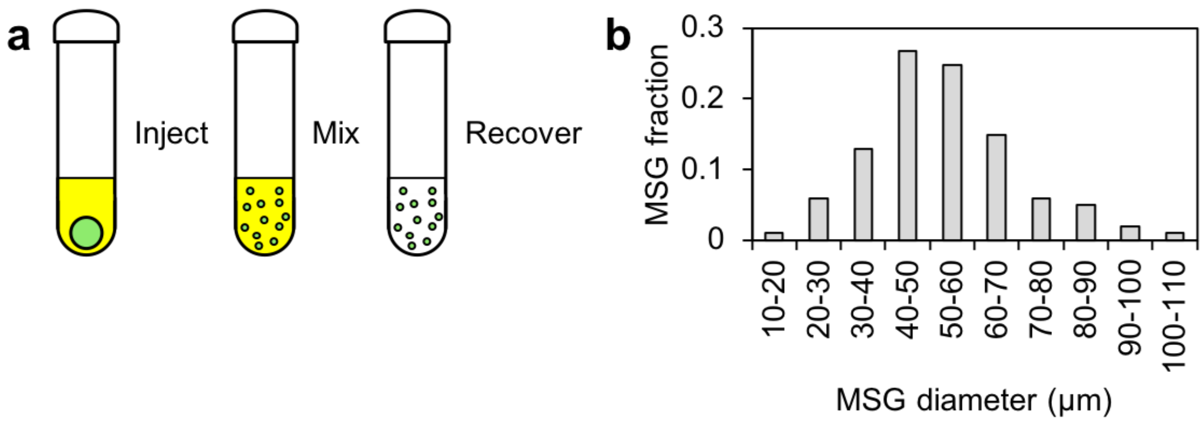


**Supplementary Figure 4.** Production and characterization of polydisperse hydrogel MSGs. (**a**) A two-phase oil/water immiscible system was used for the facile fabrication of hydrogel microspheres. Polyacrylamide pre-polymer with fluorescein methacrylate monomers were mechanically dispersed in an immiscible kerosene phase and allowed to polymerize under gentle stirring. (**b**) Size distribution of recovered microspheres indicate normal distribution of sizes with a mean diameter of ~50 μm.

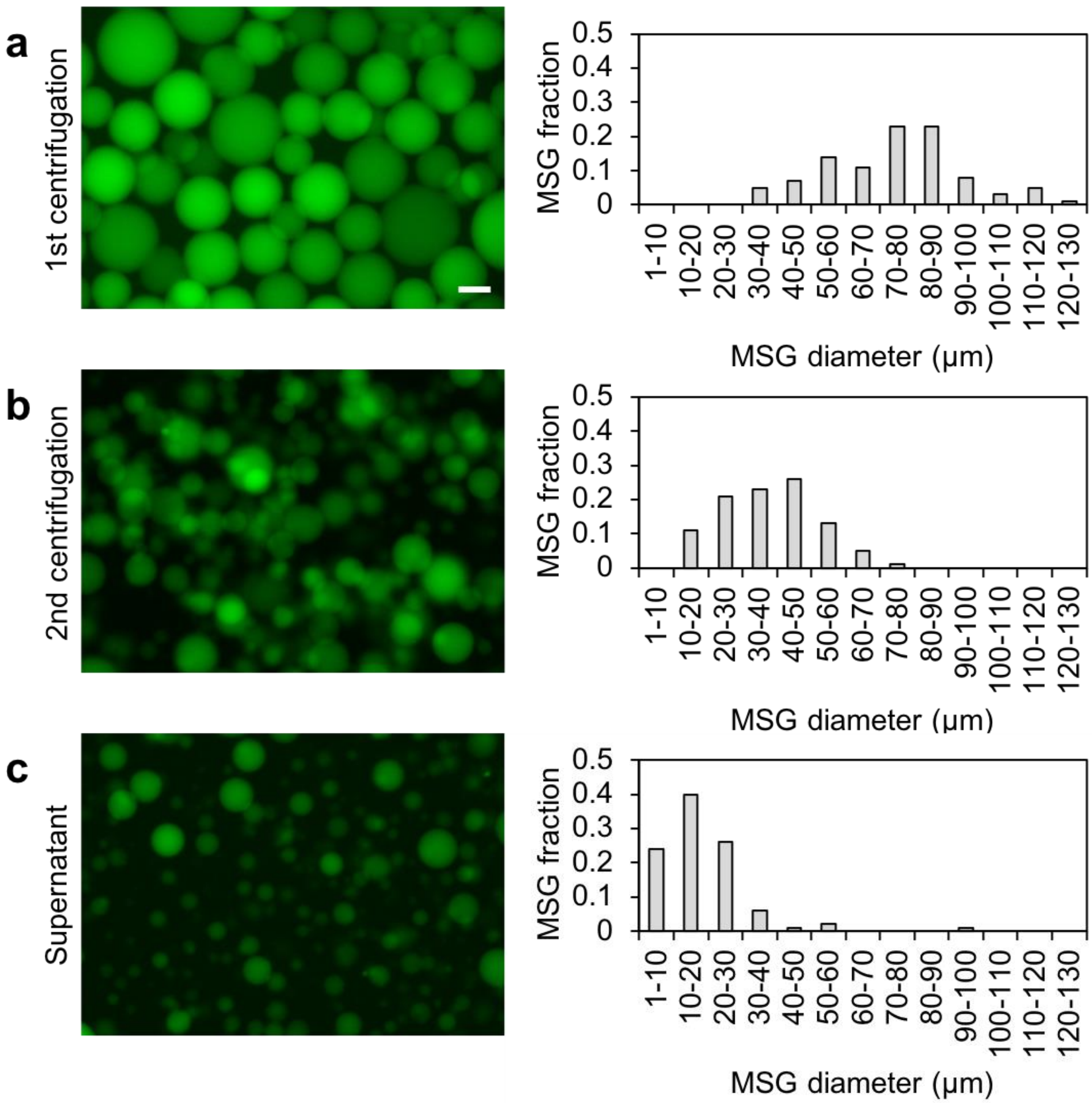


**Supplementary Figure 5.** Size separation of polydisperse hydrogel MSGs by sequential centrifugation. (**a**) Sequential centrifugation steps can be used to separate smaller hydrogel microspheres (scale bar = 50 μm), (**b**) as characterized by decreasing mean diameters, n = 100.

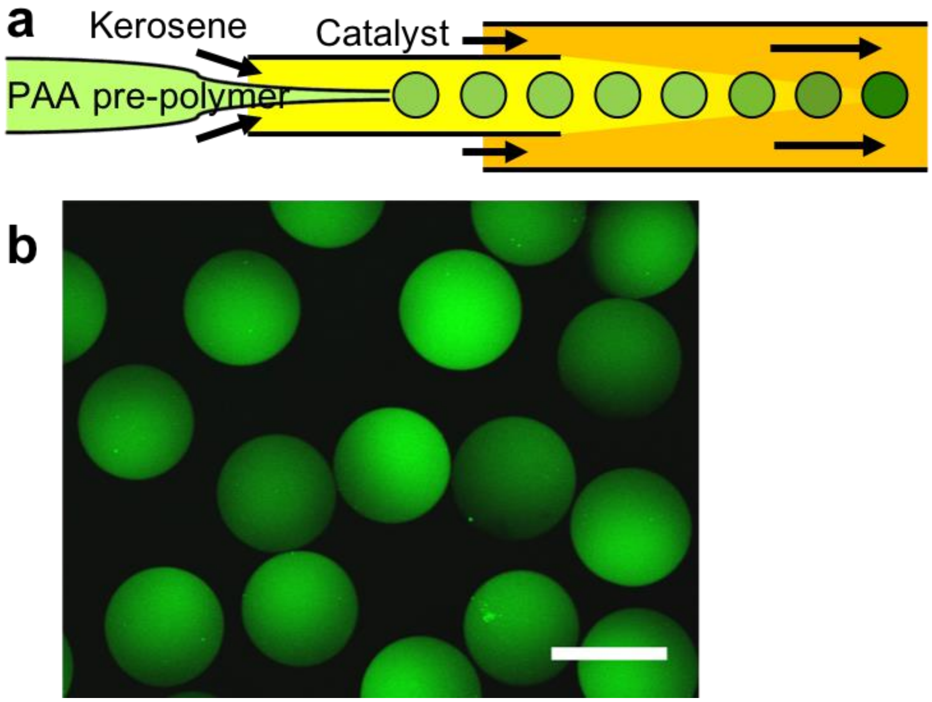


**Supplementary Figure 6.** Production of monodispersed hydrogel MSGs via microfluidic droplet generation. (**a**) A microfluidic droplet generator system consisting of a pulled circular micropipette inserted into a square glass tube was used to synthesize hydrogel microspheres of relatively uniform size. Droplets of polyacrylamide pre-polymer with fluorescein methacrylate monomers were generated in kerosene. A catalyst was added downstream of the droplet generation site, and hydrogel microspheres were allowed to polymerize. (**b**) The process enables the rapid production of a large number of uniform hydrogel microspheres (scale bar = 200 µm).

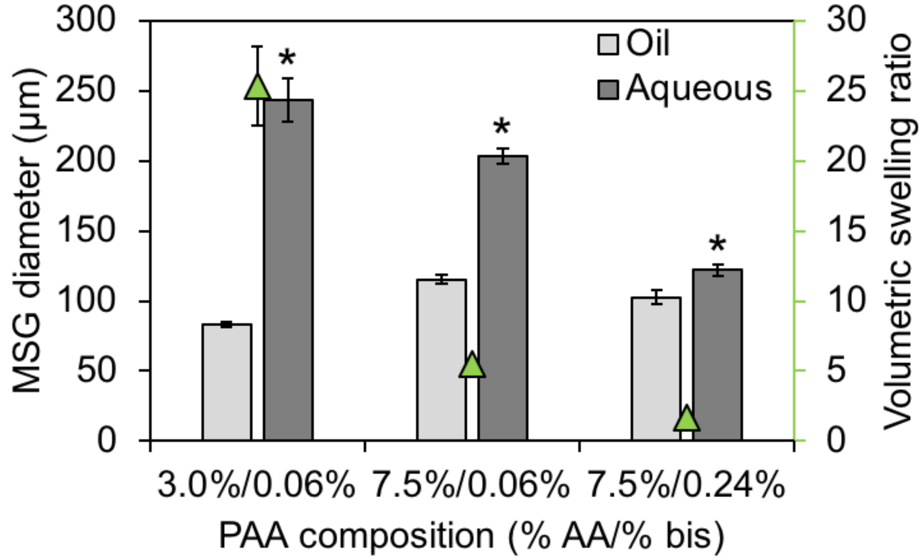


**Supplementary Figure 7.** Volumetric swelling ratio of hydrogel MSGs in oil and aqueous phases. The soft hydrogels developed here swell significantly in aqueous medium, making it challenging to fabricate very small MSGs of uniform size. Data reported as mean ± standard deviation, $n > 20$, * indicates $p < 0.05$ (one-way ANOVA with Tukey post-hoc pairwise comparisons).

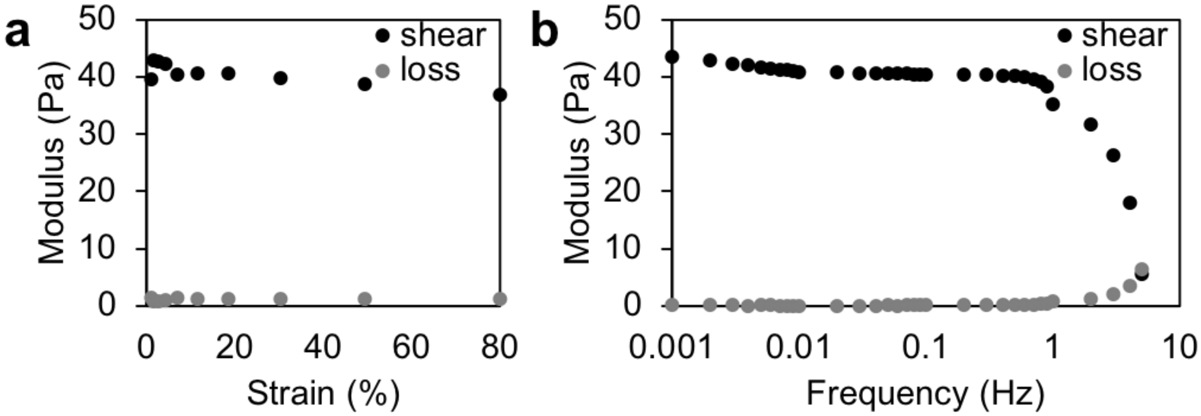


**Supplementary Figure 8.** Shear rheometry characterization of bulk, fluorescently-labelled polyacrylamide hydrogels. These bulk measurements demonstrate linear elastic material properties with negligible loss modulus (**a**) over large strain range (data repeated in main manuscript Fig. 2a) and (**b**) for load frequencies less than 1 Hz. For frequencies greater than 1 Hz, the reduced shear modulus is likely due to slippage of the hydrogel on the rheometer plates. However, frequencies greater than 1 Hz are unlikely to be relevant to the current application of MSGs in multicellular spheroids.

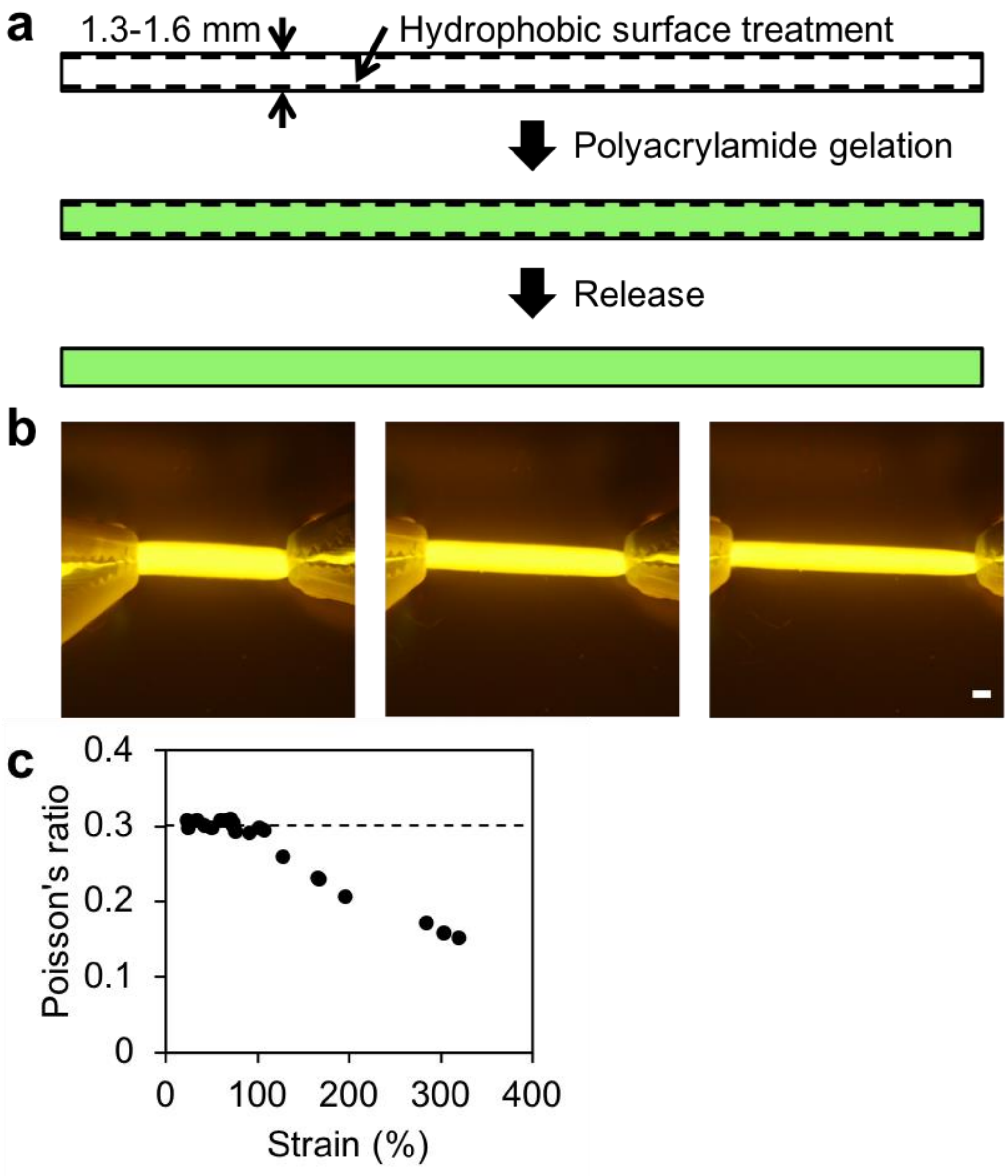


**Supplementary Figure 9.** Measurement of Poisson's ratio of the fluorescently-labelled polyacrylamide hydrogel formulations used in this work. (**a**) Polyacrylamide hydrogel "strings" were fabricated within glass capillaries (internal diameter of 1.3-1.6 mm) that had been pre-treated to be hydrophobic. Following gelation, polyacrylamide hydrogel strings were released from the glass capillary and swelled for 24 hours before (**b**) stretching axially (scale bar = 1 mm) under a fluorescent dissecting microscope. The deformations in the transverse and axial directions were measured to compute the Poisson's ratio which (**c**) remains constant for strains up to 120% (data repeated in main manuscript Fig. 2b).

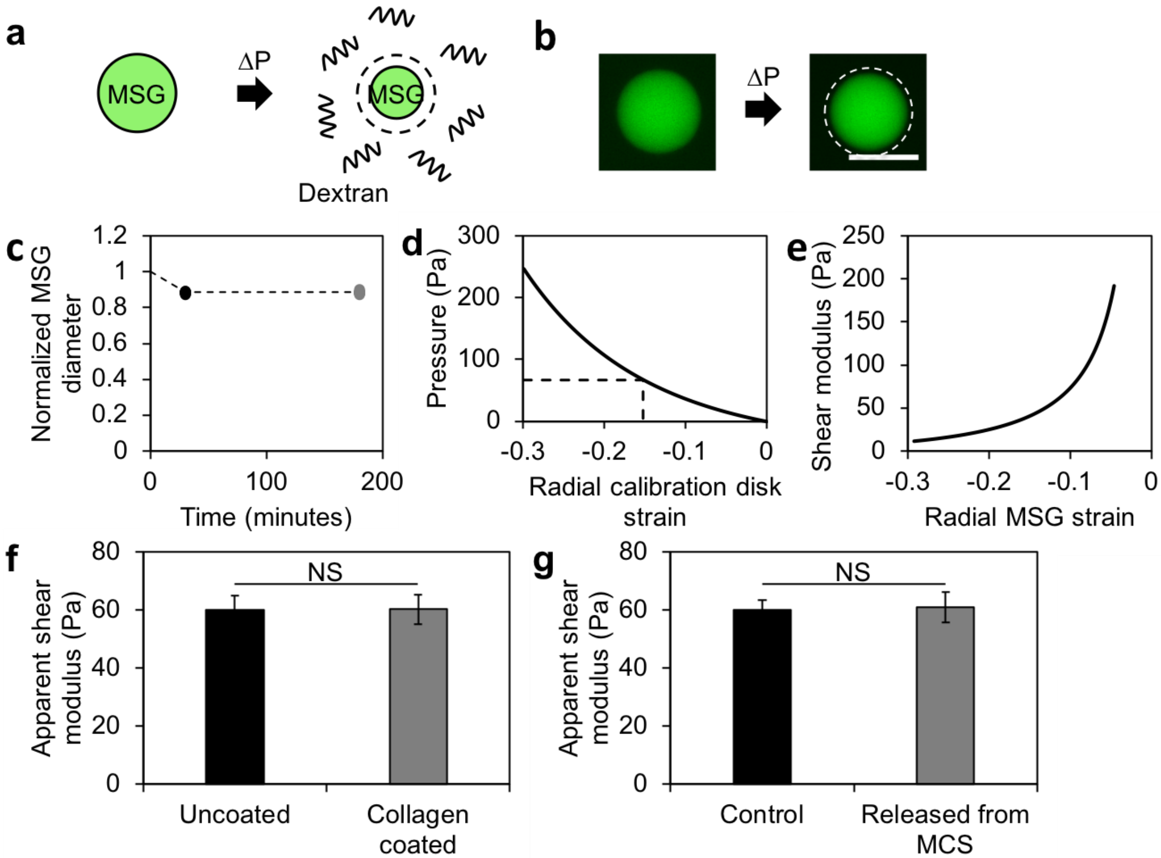


**Supplementary Figure 10.** Measurement of MSG mechanical properties by application of osmotic pressure. An aqueous solution of long-chain dextran (500 kDa) was used to exert an osmotic pressure on polyacrylamide hydrogels. The dextran polymer chains are too large to enter the polyacrylamide pores, and are therefore excluded from the hydrogel. The osmotic pressure differential forces water out of the MSG, which deforms in proportion to the MSG mechanical compliance. (**a**) A schematic representation and (**b**) fluorescent microscope images (scale bar = 50 μm) depicting hydrogel contraction when exposed to 100 mg/mL of dextran solution. (**c**) MSG sizes remain constant after 3 hours in the dextran solution, confirming that dextran chains are excluded from the polymer matrix (n = 19). The system was calibrated against osmotic pressure-induced deformation of a bulk disk-shaped polyacrylamide hydrogel sample (diameter = 13 mm) for which the shear modulus was established using conventional shear rheometry. (**d**) A finite element simulation was developed to determine the effective osmotic pressure generated by a 100 mg/mL solution of dextran. The parametric sweep of external pressures on samples was used to determine that 100 mg/mL of dextran exerts 67 Pa pressure on the hydrogel surface. Next, this osmotic pressure value was applied to (**e**) a parametric sweep of shear modulus in the isotropic compression of a spherical MSG. (**f**) Osmotic pressure measurements on MSGs indicates that collagen coating does not significantly alter mechanical rigidity of the MSG (n = 24, p = 0.782). (**g**) No significant differences were found between coated MSGs (control) and MSGs that had been removed from spheroids after two days of culture by detergent-based extraction (released), demonstrating that MSG properties remain constant even after embedding within the tissue of interest (n = 16-19, p = 0.837). All data reported as mean ± standard deviation. NS indicates no significant differences (one-way ANOVA with Tukey post-hoc pairwise comparisons).

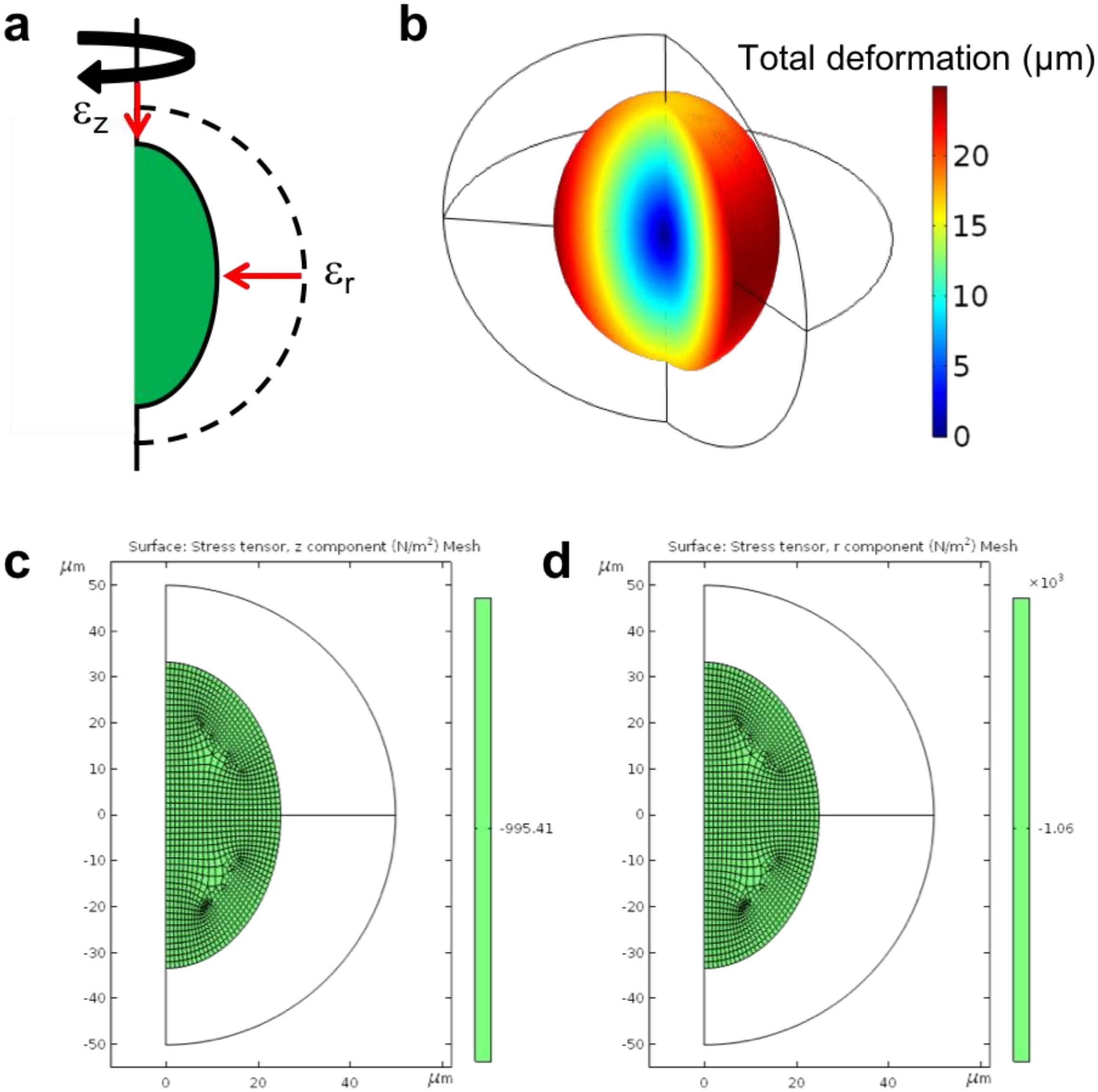


**Supplementary Figure 11.** Finite element model to simulate multiaxial MSG deformation. (**a**) Schematic of the two-dimensional axisymmetric model along with strain conditions applied throughout the bead domain. (**b**) Representative image of a partially revolved axisymmetric MSG bead deforming under -0.33 axial strain and -0.5 radial strain domain conditions. Corresponding (**c**) axial and (**d**) radial stresses are confirmed to be uniform throughout the MSG, consistent with the assumption of viscous flow in the surrounding tissue.

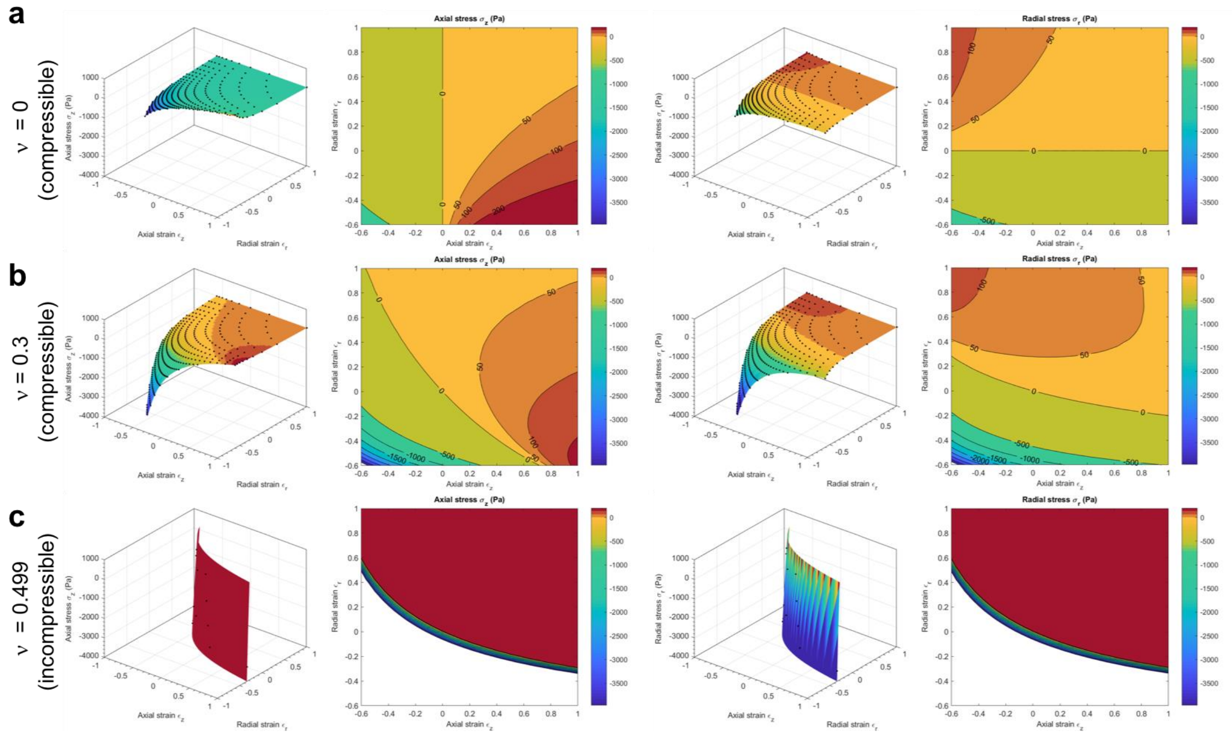


**Supplementary Figure 12.** Compressibility of the hydrogel is an important parameter in generating unique solutions for axial and radial stresses based on measured MSG deformation. Finite element simulations relating axial (z) and radial (r) stresses with axial and radial strains for (**a**) perfectly compressible (ν = 0), (**b**) actual (ν = 0.3) and (**c**) incompressible (ν = 0.499) materials. For perfectly compressible materials, strains in the axial and radial directions are only weakly coupled to radial and axial stresses respectively. On the other end of the spectrum, as the material approaches (**c**) incompressibility (ν = 0.499), microsphere deformations cannot be resolved into unique combinations of axial and radial stress. Hence, the use of compressible materials enables the measurement of both isotropic and anisotropic stress components in the system.

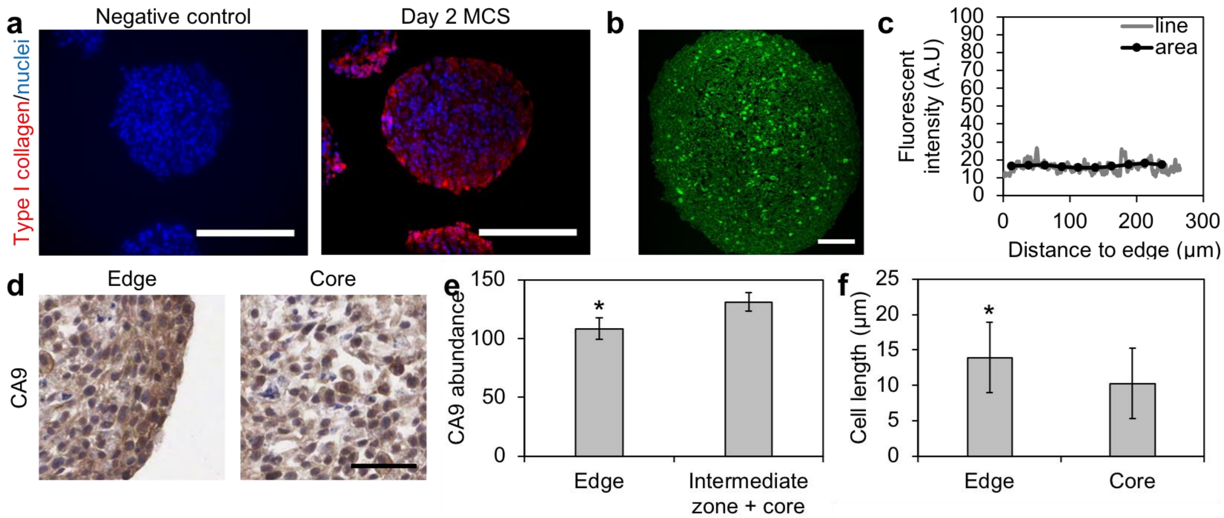


**Supplementary Figure 13.** Characterization of MCS structure 48 hours after formation. (**a**) Type I collagen fluorescent immunostaining on sectioned MCS confirms that HS-5 fibroblasts secrete Type I collagen over 2 days of culture (scale bar = 250 µm). Negative control performed without primary antibody confirms that the signal detected is not a result of non-specific binding. (**b, c**) Second harmonic imaging of collagen shows no spatial variation in ECM organization within spheroid sections. (**b**) Second harmonic imaging of mature collagen on sectioned spheroids indicates no spatial variations (scale bar = 100 µm). (**c**) Quantification of fluorescence intensity along a line segment and normalized to quantified area shows no variation in mature collagen content within MCS. (**d, e**) The core of spheroid cultures does not exhibit hypoxia as indicated by immunohistochemical analysis for carbonic anhydrase 9 (CA9), a marker of hypoxia. (**d**) A representative immunohistochemical section is shown (scale bar = 50 µm). (**e**) Immunohistochemical analysis shows similar abundance of CA9 in cells located in the periphery and the core of the spheroid, indicating an absence of an oxygen gradient. Data reported as mean ± standard deviation, n = 13, * indicates $p < 0.001$ (one-way ANOVA with Tukey post-hoc pairwise comparisons). (f) Characterization of cell elongation in H&E stained spheroid sections. Data reported as mean ± standard deviation, n = 30 over 3 spheroids, * indicates $p < 0.001$ (one-way ANOVA with Tukey post-hoc pairwise comparisons).

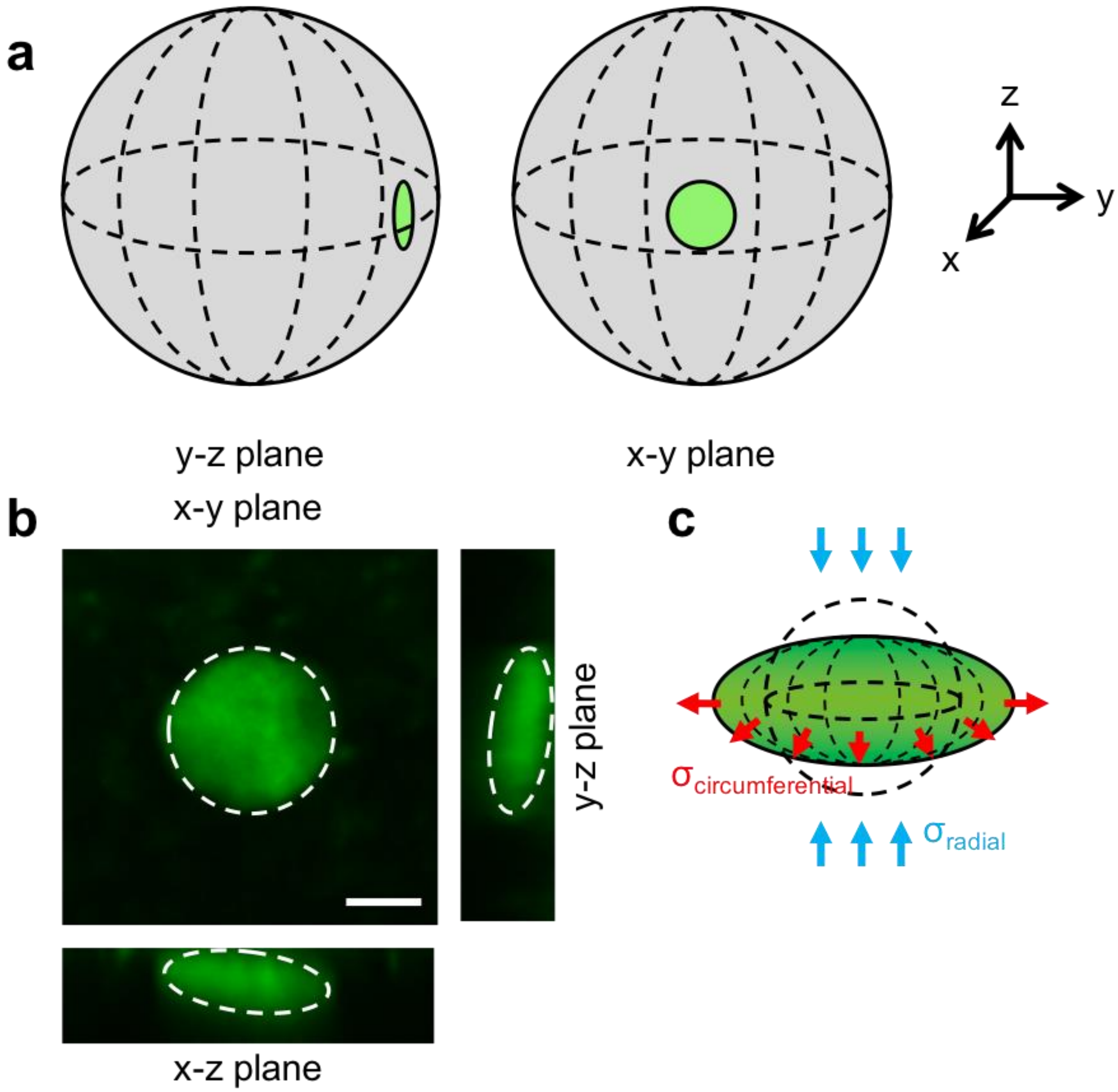


**Supplementary Figure 14.** Reconstructed confocal images of MSGs embedded at the periphery of the MSG confirms symmetric deformaton of the MSGs within spheroid cultures. (a) Schematic representation of the MSG location within the spheroids, and (b) reconstructed confocal images of MSGs close to the surface show deformations as expected based on spherical symmetry (scale bar = 25 μm), (c) The ‘pancake’-like morphologies adopted demonstrate two main axes of uniform deformation (radial and circumferential), arising from compressive radial stress and tensional circumferential stress.

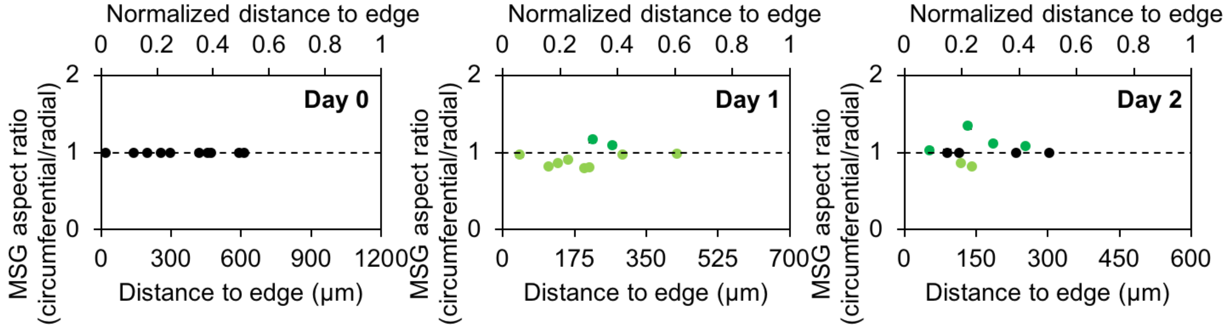


**Supplementary Figure 15.** Measurement of circumferential and radial microsphere strains indicate some spatial pattern in microsphere orientation within blebbistatin treated MCS in the first 24 hours. This preferential orientation is lost by day 2 in blebbistatin treated MCS cultures. Data reported as mean ± standard deviation for measurement error.

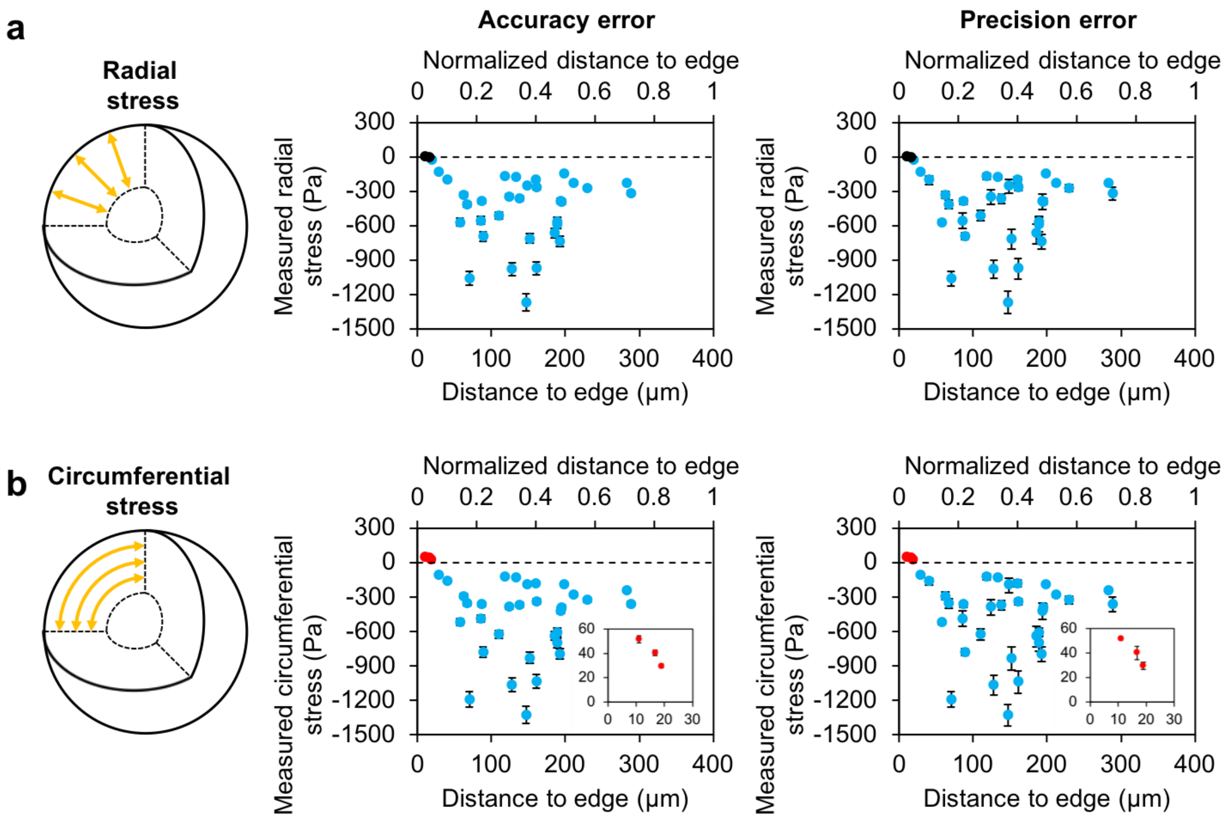


**Supplementary Figure 16.** Comparison of MSG errors associated with uncertainties in MSG modulus (accuracy) and strain measurement error (precision) in the (**a**) radial and (**b**) circumferential directions at day 2 of culture. Red data points represent tensional stress measurements, blue data points represent compressional stress measurements, and black data points represent stress measurements close to zero (-10 Pa to +10 Pa). Insets depict closer view of measured tensional stresses. Accuracy errors correspond to errors of 6% in stress readings, while precision errors were generated based on Monte Carlo simulations of error assuming a Gaussian normal distribution of values for repeated measurements of radial and circumferential bead dimensions. Both errors are combined and reported in the main manuscript figures (Fig. 4).

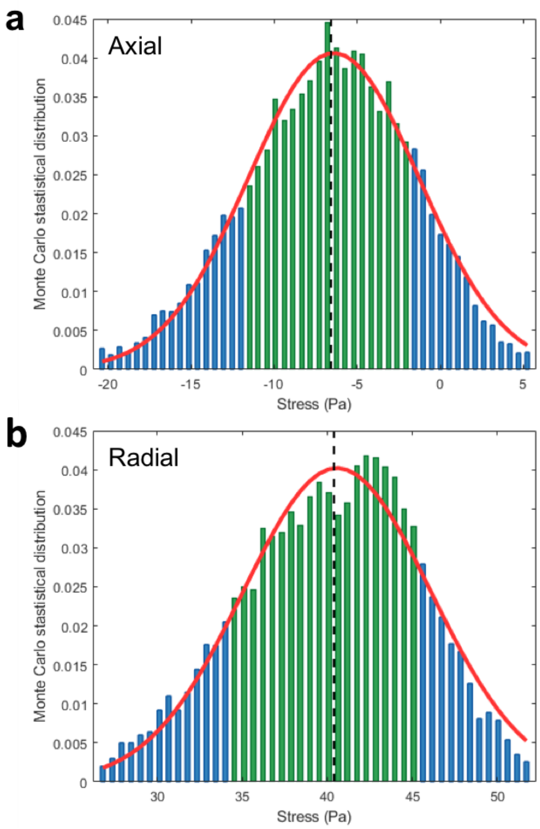


**Supplementary Figure 17.** Representative bar graphs of Monte Carlo estimates in stress measurement uncertainties arising from errors in measurement of MSG deformation. Repeated measurement of MSG dimensions was used to estimate the error in analysis of MSG size along the axial and radial axes. Assuming a Gaussian normal distribution of measurements in both the radial and circumferential axes for each data point, 10,000 randomly generated deformation values were converted to stresses through the non-linear interpolation function described in Fig. 2e, f. (**a, b**) Representative datasets from (**a**) axial and (**b**) radial stress Monte Carlo statistical distributions for a single axial compression-radial tension MSG data point (-6.50 Pa in the axial direction; +40.46 Pa in the radial direction). Mean stress values (dashed line) and their respective 95% confidence intervals (green section) are obtained empirically from the randomly generated dataset around each point. Similar curves were generated for every datapoint analyzed, and the 95% confidence intervals for each point are plotted as estimates of error in Supplementary Figure 16. These errors are then combined with errors in systemic accuracy to determine the total measurement error, values reported in Fig. 4, and in supplemental tables.

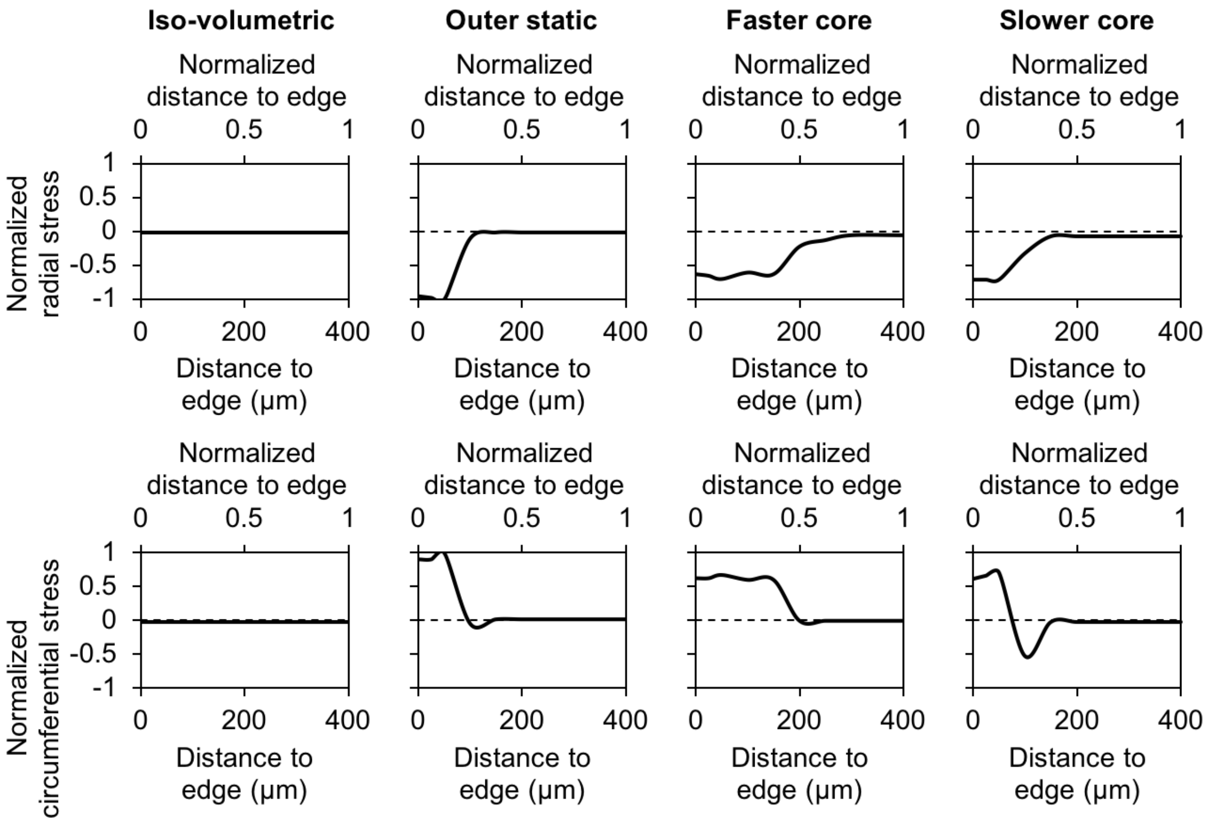


**Supplementary Figure 18.** Finite element model to simulate cell-generated mechanical stresses within MCS cultures driven by differences in cell proliferation. Finite element simulations show internal stress profiles generated with (1) iso-volumetric growth in the edge, intermediate zone, and core regions; (2) a non-proliferative edge with the intermediate zone and core growing at the same rate; (3) a non-proliferative edge with the core growing faster than the intermediate zone; and (4) a non-proliferative edge with the core growing slower than the intermediate zone. The stress profiles indicate that a non-proliferating edge is required to obtain a shell of tension in the circumferential direction around the outer layer of the MCS, as the static edge confines the growing internal layers of the spheroid, much like the walls of an inflating balloon. Mismatches in growth between the intermediate zone and core generate different stress profiles, where a peak in compression can only be obtained when the core is growing at a slower rate than the intermediate zone.

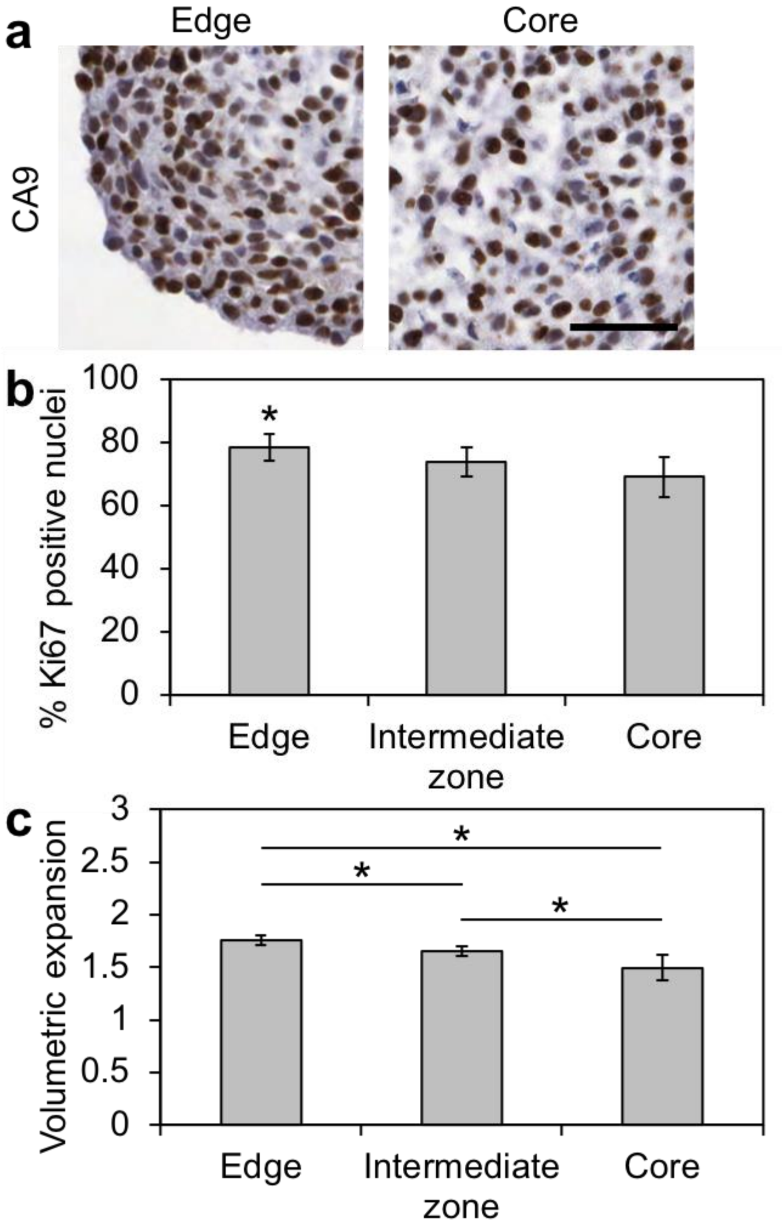


**Supplementary Figure 19.** The intermediate zone of the spheroid does not exhibit maximal cell proliferate rate by immunohistochemical analysis of Ki67, a marker of cell proliferation. (**a**) A representative immunohistochemical section is shown (scale bar = 50 μm). (**b**) Immunohistochemical analysis shows significantly higher percentage of cells positive for nuclear Ki67 in the periphery compared to the core of the spheroid, suggesting an increased rate of proliferation towards the edge of the spheroid (scale bar = 50 μm). Data reported as mean ± standard deviation, n = 11, * indicates $p < 0.05$ when compared to other spatial locations (one-way ANOVA with Tukey post-hoc pairwise comparisons). (**c**) Volumetric expansion after one cycle of cell division calculated based on nuclei packing and Ki67 staining results. Data reported as mean ± standard deviation, n = 9, * indicates $p < 0.05$ (one-way ANOVA with Tukey post-hoc pairwise comparisons).

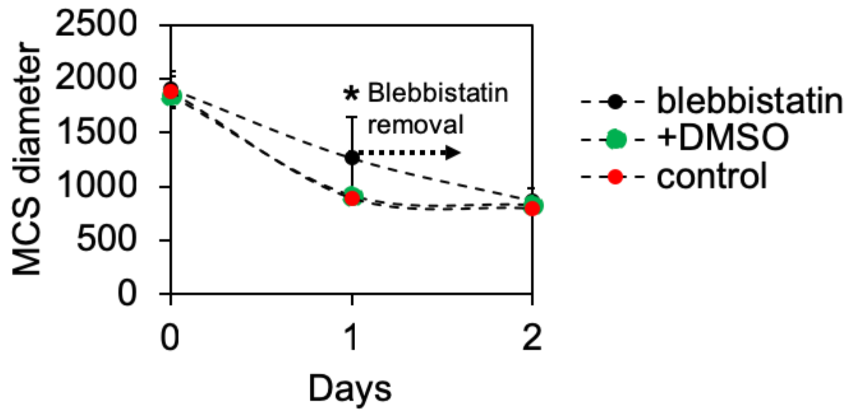


**Supplementary Figure 20**. Confirmation of blebbistatin activity through quantification of spheroid size. Compaction is significantly reduced in MCS when actomyosin contractility is inhibited with blebbistatin (day 1), but is regained when the drug is washed out (day 2). Data reported as mean ± standard deviation, n = 11, * indicates $p < 0.01$ (Student's t-test).

**Supplementary Table 1.** Radial and circumferential strains for control data set.

| | Distance to edge (μm) | Radial strain | Circumferential strain | Radial strain standard deviation | Circumferential strain standard deviation |
|---|---|---|---|---|---|
| Day 0 | 253.271667 | -0.0173117 | -0.0173117 | 0.00750415 | 0.00750415 |
| | 125.839 | 0.03100127 | 0.03100127 | 0.01065199 | 0.01065199 |
| | 22.1433333 | -0.0185852 | -0.0185852 | 0.0095284 | 0.0095284 |
| | 80.5896667 | 0.0153115 | 0.0153115 | 0.00577389 | 0.00577389 |
| | 250.139 | -0.0434611 | -0.0434611 | 0.0090087 | 0.0090087 |
| | 72.9496667 | -0.0146369 | -0.0146369 | 0.01624392 | 0.01624392 |
| | 78.2076667 | -0.023329 | -0.023329 | 0.01774364 | 0.01774364 |
| | 533.014333 | -0.0119751 | -0.0119751 | 0.01218096 | 0.01218096 |
| | 79.9646667 | -0.0024966 | -0.0024966 | 0.00878492 | 0.00878492 |
| Day 1 | 264.881667 | -0.0756392 | -0.3650069 | 0.01475975 | 0.02080695 |
| | 201.624667 | -0.4435282 | -0.2124585 | 0.01250441 | 0.0142695 |
| | 102.540667 | -0.1189901 | -0.4605942 | 0.00701969 | 0.01079038 |
| | 192.022333 | -0.2914491 | -0.4571806 | 0.01583851 | 0.01248298 |
| | 122.896667 | -0.4644802 | -0.1467778 | 0.0301295 | 0.00860798 |
| | 142.887333 | -0.4953367 | -0.0065193 | 0.00939172 | 0.00809539 |
| | 215.912333 | -0.0337602 | -0.3270834 | 0.001718 | 0.01150695 |
| | 112.064 | -0.1931875 | -0.3890554 | 0.0206755 | 0.00389932 |
| | 163.003667 | -0.1452642 | -0.4215483 | 0.01621957 | 0.0095584 |
| | 146.594333 | -0.177023 | -0.4728582 | 0.02426695 | 0.00460169 |
| | 140.748 | -0.1308068 | -0.4913635 | 0.02469393 | 0.01827656 |
| | 142.519 | -0.2168688 | -0.3912013 | 0.01278379 | 0.02710338 |
| | 134.803333 | -0.3127343 | -0.2784181 | 0.00849512 | 0.01562575 |
| | 155.406 | -0.5408411 | -0.38305 | 0.00354685 | 0.02167709 |
| | 18.788 | -0.1664079 | 0.12768318 | 0.0128192 | 0.02533022 |
| | 293.869333 | -0.2016779 | -0.2935707 | 0.0148574 | 0.01092408 |
| | 319.972 | -0.3827587 | -0.1639899 | 0.00870317 | 0.01494147 |
| Day 2 | 188.8285 | -0.2580223 | -0.4048553 | 0.02098765 | 0.0081292 |
| | 195.138667 | -0.3040303 | -0.3072777 | 0.01295648 | 0.01260982 |
| | 88.716 | -0.2227406 | -0.4594171 | 0.01186624 | 0.00509735 |
| | 146.8565 | -0.3639815 | -0.4997769 | 0.02346986 | 0.00832615 |
| | 70.0875 | -0.2281152 | -0.5271602 | 0.01903957 | 0.00670429 |
| | 124.007 | -0.2009152 | -0.3465628 | 0.03298533 | 0.02770151 |
| | 86.7036667 | -0.3705685 | -0.2628322 | 0.0162228 | 0.00719932 |
| | 57.3656667 | -0.4689408 | -0.2761605 | 0.00528345 | 0.00596835 |
| | 138.430333 | -0.2861065 | -0.3040828 | 0.00647076 | 0.02165226 |
| | 40.2276667 | -0.3510402 | -0.1272162 | 0.04559503 | 0.01905851 |
| | 10.9856667 | -0.2148388 | 0.31090689 | 0.0158255 | 0.00763435 |
| | 85.6476667 | -0.504119 | -0.2404744 | 0.01875568 | 0.02455746 |
| | 67.1053333 | -0.4622995 | -0.2061528 | 0.00837447 | 0.02187356 |
| | 160.014333 | -0.2967276 | -0.1737487 | 0.02129463 | 0.02410194 |
| | 29.206 | -0.2486057 | -0.1164766 | 0.01321434 | 0.01303668 |
| | 282.744 | -0.1935859 | -0.2687895 | 0.01394602 | 0.00398711 |
| | 288.575667 | -0.1706106 | -0.3447979 | 0.02672242 | 0.02790839 |
| | 127.933667 | -0.2815952 | -0.4925533 | 0.00332189 | 0.0138056 |
| | 109.956333 | -0.1099068 | -0.4578969 | 0.0217457 | 0.01095201 |
| | 192.460667 | -0.2794271 | -0.4438034 | 0.02203337 | 0.01126994 |
| | 148.156333 | -0.4242247 | -0.1161216 | 0.02569421 | 0.05658027 |
| | 189.080333 | -0.1426186 | -0.4670056 | 0.0267774 | 0.01341946 |
| | 62.473 | -0.3967844 | -0.2068374 | 0.01197061 | 0.01966358 |
| | 151.817667 | -0.1729637 | -0.4856882 | 0.02108204 | 0.01870056 |
| | 160.749333 | -0.3158537 | -0.4755891 | 0.00907175 | 0.01540138 |
| | 193.553667 | -0.2383188 | -0.3461599 | 0.01847675 | 0.0309486 |
| | 198.174 | -0.0764169 | -0.2676159 | 0.02499724 | 0.00517769 |
| | 160.980333 | -0.0868809 | -0.3623651 | 0.01908261 | 0.01223852 |
| | 118.081667 | -0.3606838 | -0.0797439 | 0.02692123 | 0.02829732 |
| | 133.631667 | -0.3666899 | -0.087223 | 0.01032526 | 0.02177059 |
| | 18.941 | -0.2678937 | 0.20217184 | 0.03220038 | 0.00766611 |
| | 185.406 | -0.4363358 | -0.3340389 | 0.0146086 | 0.02669782 |
| | 16.6946667 | -0.2225128 | 0.24081644 | 0.01776937 | 0.02971592 |
| | 229.6955 | -0.1318971 | -0.3409722 | 0.01519917 | 0.01715384 |
| | 211.6955 | -0.1148664 | -0.3214346 | 0.01007977 | 0.01006305 |

**Supplementary Table 2.** Radial and circumferential stresses for control data set.

| | Distance to edge (um) | Radial stress (Pa) | Circumferential stress (Pa) | (-) Radial stress standard deviation (Pa) | (+) Radial stress standard deviation (Pa) | (-) Circumferential stress standard deviation (Pa) | (+) Circumferential stress standard deviation (Pa) |
|---|---|---|---|---|---|---|---|
| Day 0 | 253.271667 | -7.301111 | -7.46598 | 2.673557 | 2.593557 | 3.083422 | 3.04337 |
| | 125.839 | 10.867287 | 10.744592 | 3.087121 | 2.934217 | 3.466865 | 3.361118 |
| | 22.1433333 | -7.862515 | -7.982986 | 3.387298 | 3.303862 | 3.817699 | 3.748761 |
| | 80.5896667 | 5.485827 | 5.396788 | 1.772409 | 1.794597 | 1.9167 | 1.947585 |
| | 250.139 | -19.706897 | -19.664205 | 4.412946 | 4.344097 | 4.804758 | 4.486302 |
| | 72.9496667 | -6.208612 | -6.239468 | 5.412413 | 5.225729 | 6.12386 | 5.721876 |
| | 78.2076667 | -9.84552 | -10.047527 | 6.671968 | 5.801549 | 7.252188 | 6.693407 |
| | 533.014333 | -5.048624 | -5.117344 | 3.832863 | 3.825252 | 4.514839 | 4.266862 |
| | 79.9646667 | -1.076698 | -1.120348 | 2.643903 | 2.435971 | 3.093488 | 2.799602 |
| Day 1 | 264.881667 | -261.75762 | -334.43597 | 38.035727 | 52.732491 | 47.45485 | 64.940733 |
| | 201.624667 | -398.18737 | -344.16315 | 30.991038 | 53.707327 | 51.267018 | 50.46976 |
| | 102.540667 | -531.06431 | -644.70631 | 37.356059 | 68.0837 | 65.569626 | 81.289143 |
| | 192.022333 | -819.67546 | -879.47562 | 69.837459 | 117.734797 | 111.592762 | 125.020398 |
| | 122.896667 | -327.89236 | -260.0256 | 41.668457 | 60.388879 | 54.455746 | 47.888101 |
| | 142.887333 | -216.22689 | -127.97752 | 11.201104 | 23.744437 | 23.19474 | 17.009063 |
| | 215.912333 | -179.82457 | -245.99289 | 13.225495 | 23.783057 | 24.064874 | 32.007787 |
| | 112.064 | -429.16753 | -484.49093 | 27.561167 | 52.50293 | 51.578255 | 51.567937 |
| | 163.003667 | -450.84812 | -534.5096 | 33.832836 | 59.855218 | 56.470742 | 66.421246 |
| | 146.594333 | -667.01141 | -772.09647 | 47.534088 | 86.904745 | 83.335314 | 87.493245 |
| | 140.748 | -663.59051 | -796.52014 | 93.714852 | 132.293223 | 119.533007 | 152.127711 |
| | 142.519 | -465.21639 | -515.17424 | 75.8833 | 103.687071 | 94.450046 | 118.301684 |
| | 134.803333 | -347.38045 | -339.36633 | 29.590402 | 49.473281 | 45.958238 | 51.596852 |
| | 155.406 | -1171.3065 | -1112.9573 | 125.031734 | 193.401521 | 180.029051 | 194.988333 |
| | 18.788 | -12.45476 | 20.202178 | 5.393404 | 5.971468 | 5.493387 | 7.784411 |
| | 293.869333 | -263.00106 | -283.75706 | 20.521845 | 35.563459 | 34.304281 | 37.504438 |
| | 319.972 | -261.90548 | -217.68424 | 19.624759 | 34.776661 | 32.433646 | 33.587842 |
| Day 2 | 188.8285 | -561.74726 | -606.59078 | 74.345071 | 72.994292 | 74.597857 | 73.415059 |
| | 195.138667 | -389.21268 | -390.04614 | 51.764252 | 50.066928 | 53.518171 | 51.114409 |
| | 88.716 | -692.93029 | -775.17568 | 70.596834 | 69.651415 | 75.706811 | 73.828534 |
| | 146.8565 | -1265.8421 | -1324.417 | 176.092648 | 168.148629 | 175.724862 | 168.794673 |
| | 70.0875 | -1058.3039 | -1187.6877 | 129.106966 | 124.482019 | 136.100324 | 131.188514 |
| | 124.007 | -346.58811 | -383.7132 | 88.498538 | 75.11601 | 95.310407 | 80.613553 |
| | 86.7036667 | -388.38562 | -362.7006 | 47.290177 | 45.288914 | 43.406404 | 41.605168 |
| | 57.3656667 | -569.80526 | -517.59844 | 50.362442 | 50.991774 | 47.374011 | 47.727092 |
| | 138.430333 | -363.20447 | -367.80412 | 63.61905 | 59.24869 | 69.366227 | 64.504504 |
| | 40.2276667 | -198.99379 | -158.16559 | 53.440548 | 45.903549 | 42.860863 | 37.126817 |
| | 10.9856667 | 2.728722 | 51.664435 | 2.758705 | 2.605397 | 4.11539 | 4.110623 |
| | 85.6476667 | -554.0227 | -484.98441 | 104.268008 | 95.329613 | 99.417808 | 92.712085 |
| | 67.1053333 | -413.91522 | -353.47635 | 65.203254 | 59.960379 | 64.104445 | 58.100034 |
| | 160.014333 | -200.96727 | -177.51766 | 40.941258 | 37.310014 | 40.547429 | 37.110482 |
| | 29.206 | -126.87073 | -104.83445 | 18.090161 | 17.607321 | 17.131145 | 16.499581 |
| | 282.744 | -224.40981 | -240.62926 | 24.851578 | 23.482379 | 23.773275 | 22.704362 |
| | 288.575667 | -314.27931 | -357.63049 | 78.688965 | 68.147019 | 88.249107 | 76.277875 |
| | 127.933667 | -978.05519 | -1061.7975 | 138.80166 | 131.97834 | 152.938279 | 145.161453 |
| | 109.956333 | -510.53929 | -624.53872 | 76.202414 | 73.624658 | 85.597569 | 81.837102 |
| | 192.460667 | -736.68699 | -793.52568 | 111.211723 | 105.124773 | 114.388202 | 109.361181 |
| | 148.156333 | -249.70145 | -189.79308 | 84.616506 | 69.884388 | 84.508178 | 69.713043 |
| | 189.080333 | -587.96949 | -699.56491 | 100.321726 | 94.225167 | 109.655728 | 104.467225 |
| | 62.473 | -331.50159 | -289.57881 | 52.55099 | 49.866248 | 51.475102 | 48.783613 |
| | 151.817667 | -712.22459 | -827.89834 | 135.846737 | 122.513602 | 152.064473 | 139.094313 |
| | 160.749333 | -970.83425 | -1032.3334 | 150.399661 | 140.79986 | 162.008984 | 151.48817 |
| | 193.553667 | -387.43063 | -415.59427 | 93.288523 | 81.157794 | 103.267326 | 90.685279 |
| | 198.174 | -145.45285 | -184.15277 | 24.225872 | 22.711096 | 22.790903 | 21.894121 |
| | 160.980333 | -268.25797 | -337.4293 | 41.56183 | 41.131887 | 47.77239 | 46.948338 |
| | 118.081667 | -167.9813 | -119.41575 | 38.930277 | 35.06345 | 35.279741 | 31.066598 |
| | 133.631667 | -177.73477 | -128.68484 | 29.776894 | 27.4939 | 28.42619 | 26.117421 |
| | 18.941 | -21.819972 | 29.703175 | 9.180939 | 8.412283 | 4.856412 | 4.423935 |
| | 185.406 | -664.25138 | -633.86438 | 132.773095 | 119.351704 | 136.021535 | 120.612126 |
| | 16.6946667 | -6.489743 | 40.463765 | 5.828272 | 5.302946 | 8.2697 | 7.276722 |
| | 229.6955 | -272.29484 | -322.97951 | 46.735394 | 43.332894 | 54.426264 | 50.12556 |
| | 211.6955 | -230.56426 | -278.4297 | 29.40033 | 28.336532 | 34.33804 | 33.707544 |

**Supplementary Table 3.** Radial and circumferential strains for blebbistatin data set.

| | Distance to edge (μm) | Radial strain | Circumferential strain | Radial strain standard deviation | Circumferential strain standard deviation |
|---|---|---|---|---|---|
| Day 0 | 589.337333 | -0.0036178 | -0.0036178 | 0.01918289 | 0.01918289 |
| | 138.919 | -0.0025079 | -0.0025079 | 0.01554925 | 0.01554925 |
| | 256.589333 | -0.021659 | -0.021659 | 0.00523918 | 0.00523918 |
| | 470.431667 | -0.0119578 | -0.0119578 | 0.01186768 | 0.01186768 |
| | 418.662 | -0.0001081 | -0.0001081 | 0.02322107 | 0.02322107 |
| | 611.276 | -0.0156326 | -0.0156326 | 0.01735828 | 0.01735828 |
| | 198.466333 | -0.0061013 | -0.0061013 | 0.01056779 | 0.01056779 |
| | 19.0333333 | 0.00388331 | 0.00388331 | 0.00672608 | 0.00672608 |
| | 455.868 | -0.0024674 | -0.0024674 | 0.00427361 | 0.00427361 |
| | 295.665 | 0.0023396 | 0.0023396 | 0.01474246 | 0.01474246 |
| Day 1 | 267.940333 | -0.1459092 | -0.0648114 | 0.02909371 | 0.03918094 |
| | 197.882333 | -0.1331089 | -0.3074382 | 0.01417008 | 0.00684715 |
| | 425.124 | -0.167206 | -0.17867 | 0.00350152 | 0.01024833 |
| | 218.567333 | -0.2468586 | -0.1183345 | 0.03166042 | 0.01812759 |
| | 158.978667 | -0.084651 | -0.1668022 | 0.02114879 | 0.01834155 |
| | 292.672 | -0.0682101 | -0.0880765 | 0.01041673 | 0.02072814 |
| | 111.107 | -0.0684003 | -0.2393817 | 0.01173793 | 0.01521672 |
| | 41.367 | -0.2342072 | -0.256783 | 0.02975877 | 0.01089485 |
| | 134.602333 | -0.1505166 | -0.2655213 | 0.01607685 | 0.01718629 |
| | 210.735 | -0.0516536 | -0.2303518 | 0.01723254 | 0.01605707 |
| Day 2 | 233.825 | -0.0610635 | -0.0610635 | 0.03067846 | 0.03067846 |
| | 140.584333 | -0.1354361 | -0.2873418 | 0.00685044 | 0.01464093 |
| | 302.595333 | -0.2047461 | -0.2047461 | 0.01497081 | 0.01497081 |
| | 113.751667 | -0.198659 | -0.198659 | 0.01453806 | 0.01453806 |
| | 89.9246667 | -0.1709642 | -0.1709642 | 0.03567907 | 0.03567907 |
| | 253.883667 | -0.1032205 | -0.0301937 | 0.00805639 | 0.01423848 |
| | 118.448667 | -0.2170043 | -0.3249506 | 0.01525382 | 0.00647636 |
| | 52.81 | -0.2141286 | -0.1879506 | 0.01686422 | 0.02845634 |
| | 132.842 | -0.3995903 | -0.1918081 | 0.01627582 | 0.02307093 |
| | 186.460333 | -0.2798243 | -0.1945363 | 0.01028737 | 0.01708143 |

**Supplementary Table 4.** Radial and circumferential stresses for blebbistatin data set.

| | Distance to edge (um) | Radial stress (Pa) | Circumferential stress (Pa) | (-) Radial stress standard deviation (Pa) | (+) Radial stress standard deviation (Pa) | (-) Circumferential stress standard deviation (Pa) | (+) Circumferential stress standard deviation (Pa) |
|---|---|---|---|---|---|---|---|
| Day 0 | 589.337333 | -1.617427 | -1.53564 | 5.830154 | 5.317222 | 6.645397 | 5.760238 |
| | 138.919 | -1.14694 | -1.117039 | 4.763156 | 4.326811 | 5.422539 | 4.694686 |
| | 256.589333 | -9.164581 | -9.272991 | 2.197596 | 2.097677 | 2.399856 | 2.306334 |
| | 470.431667 | -5.06666 | -5.135499 | 3.821231 | 3.854714 | 4.422385 | 4.421893 |
| | 418.662 | -0.221587 | -0.193348 | 6.961076 | 6.206786 | 7.976663 | 6.779683 |
| | 611.276 | -6.552472 | -6.61721 | 5.885485 | 5.487462 | 6.57209 | 6.176144 |
| | 198.466333 | -2.594393 | -2.634016 | 3.349753 | 3.308872 | 3.843778 | 3.649243 |
| | 19.0333333 | 1.383025 | 1.410119 | 1.824517 | 1.765593 | 2.202045 | 1.998116 |
| | 455.868 | -1.033383 | -1.054274 | 1.313714 | 1.264916 | 1.541055 | 1.414794 |
| | 295.665 | 0.774753 | 0.810081 | 4.262314 | 3.755217 | 4.913647 | 4.172076 |
| Day 1 | 267.940333 | -57.369712 | -46.043881 | 22.678407 | 20.125705 | 24.784701 | 22.112644 |
| | 197.882333 | -225.90097 | -265.39404 | 27.329818 | 25.980629 | 29.09932 | 28.444571 |
| | 425.124 | -125.67903 | -127.85501 | 14.864042 | 14.817605 | 16.789433 | 16.748918 |
| | 218.567333 | -127.10968 | -105.62886 | 29.076092 | 27.043713 | 25.043378 | 23.088426 |
| | 158.978667 | -79.788391 | -93.368335 | 18.454378 | 17.15671 | 20.705925 | 19.034733 |
| | 292.672 | -40.196489 | -42.995932 | 10.514124 | 10.03789 | 13.476621 | 12.283223 |
| | 111.107 | -118.26448 | -150.64298 | 20.241123 | 19.099798 | 24.998544 | 23.942445 |
| | 41.367 | -242.01016 | -247.00051 | 43.390912 | 40.622641 | 39.940205 | 37.205777 |
| | 134.602333 | -189.86537 | -213.88999 | 33.3809 | 31.325827 | 37.623777 | 35.295874 |
| | 210.735 | -102.94193 | -135.80386 | 20.372866 | 18.422001 | 24.571439 | 22.64755 |
| Day 2 | 233.825 | -29.461782 | -29.561393 | 15.18428 | 13.624754 | 16.69375 | 14.927409 |
| | 140.584333 | -203.51195 | -236.34333 | 30.316255 | 28.486122 | 36.13435 | 34.168667 |
| | 302.595333 | -167.4361 | -167.49788 | 26.342316 | 25.133887 | 27.743775 | 26.001236 |
| | 113.751667 | -157.93236 | -158.04869 | 24.702411 | 22.913386 | 25.954504 | 24.12351 |
| | 89.9246667 | -122.48514 | -122.62976 | 40.798365 | 34.944301 | 43.514874 | 37.508318 |
| | 253.883667 | -32.312682 | -22.770725 | 6.839203 | 6.282639 | 7.3087 | 7.102654 |
| | 118.448667 | -325.68243 | -352.16013 | 37.930289 | 36.787076 | 38.195174 | 36.990667 |
| | 52.81 | -158.38726 | -153.76607 | 35.760994 | 32.171951 | 39.741778 | 35.530578 |
| | 132.842 | -313.57802 | -268.79854 | 55.496495 | 52.042927 | 54.0324 | 50.381177 |
| | 186.460333 | -209.06344 | -192.22974 | 31.197826 | 30.365373 | 32.403349 | 31.062419 |